Mechanics of Single Kinesin Molecules Measured by Optical Trapping Nanometry

Hiroaki Kojima,* Etsuko Muto,* Hideo Higuchi,* and Toshio Yanagida#§
*Yanagida Biomotron Project, ERATO, JST, Mino, Osaka 562; #Department of Biophysical Engineering, Osaka University, Toyonaka, Osaka 560; and §Department of Physiology, School of Medicine, Osaka University, Osaka 565, Japan

ABSTRACT We have analyzed the mechanics of individual kinesin molecules by optical trapping nanometry. A kinesin molecule was adsorbed onto a latex bead, which was captured by an optical trap and brought into contact with an axoneme that was bound to a glass surface. The displacement of kinesin during force generation was determined by measuring the position of the beads with nanometer accuracy. As the displacement of kinesin was attenuated because of the compliance of the kinesin-to-bead and kinesin-to-microtubule linkages, the compliance was monitored during force generation and was used to correct the displacement of kinesin. Thus the velocity and the unitary steps could be obtained accurately over a wide force range. The force-velocity curves were linear from 0 to a maximum force at 10 μM and 1 mM ATP, and the maximum force was ~7 pN, which is larger by ~30% than values previously reported. Kinesin exhibited forward and occasionally backward stepwise displacements with a size of ~8 nm. The histograms of step dwell time show a monotonic decrease with time. Model calculations indicate that each kinesin head steps by 16-nm, whereas kinesin molecule steps by 8-nm.

INTRODUCTION

Kinesin is a molecular motor that transports cellular organelles along microtubules. Kinesin converts the chemical energy that is derived from ATP hydrolysis into mechanical energy for force generation, as actomyosin and dynein motors do. Recently, very powerful methods that allow the observation of the elementary process of force generation by individual motors have been developed (Ishijima et al., 1991, 1994, 1996; Svoboda et al., 1993; Finer et al., 1994). Furthermore, it is possible to observe the movement of individual fluorescent motors by fluorescence microscopy (Funatsu et al., 1995; Vale et al., 1996). Kinesin is well suited to single-molecule analysis, because kinesin molecules operate alone or in small numbers, unlike myosin and dynein, which operate in large arrays. Kinesin tends not to detach between steps, and so chains of single-molecule events can be observed (Howard et al., 1989; Svoboda et al., 1993; Vale et al., 1996).

Svoboda and co-workers (1993) and Higuchi and co-workers (1997) demonstrated that kinesin-coated beads exhibit a stepwise displacement with an amplitude of ~8 and ~16 nm, by using optical trapping nanometry. An 8-nm step coincides with the periodicity of the tubulin heterodimers in a microtubule, and a 16-nm step is generated either by the rapid succession of two 8-nm steps or a single 16-nm step. Coppin and co-workers have reported 8-nm steps, with additional 5-nm steps being observed. Thus the question arises as to the unitary step size of kinesin along a microtubule: 5, 8, or 16 nm?

The step size of kinesin molecules can be calculated from the displacement of kinesin-coated beads plus the elongation of kinesin-to-bead linkage. The elongation of kinesin-to-bead linkage was estimated from its stiffness (Svoboda and Block, 1994a; Coppin et al., 1996; Ishijima et al., 1996). In previous studies, the stiffness of kinesin-to-bead linkage was estimated under experimental conditions without ATP (Svoboda et al., 1993; Svoboda and Block, 1994a; Coppin et al., 1996). In these experiments, it was assumed that stiffness during force generation was the same as that without ATP and was independent of the level of force produced. In this paper we measured the stiffness of kinesin-to-beads linkage simultaneously with the force by applying sinusoidal oscillations to the trap position. We also improved the temporal resolution by utilizing stiff biological preparations of axoneme-kinesin, wherein the thermal fluctuations of kinesin-coated beads should be suppressed. At high temporal resolution, we only observed step sizes of 8 nm. To determine the manner in which kinesin heads move, we analyzed the dwell time of the 8-nm steps. The histograms of the dwell time showed a monotonic decrease. We simulated the dwell time by using models of kinesin heads of step 8 or 16 nm. The results of the simulations were consistent with a hand-over-hand model in which each kinesin head steps by 16 nm.

Received for publication 2 December 1996 and in final form 14 July 1997.

Address reprint requests to Dr. Hideo Higuchi, Yanagida Biomotron Project, ERATO, JST, Senba-Higashi 2-4-14, Mino, Osaka, Japan. Tel.: 81-727-28-7003; Fax: 81-727-28-7033; E-mail: higuchi@yanagida.jst.go.jp.

Hiroaki Kojima's present address is Kansai Advanced Research Center, Communications Research Laboratory, Ministry of Posts and Telecommunications 588-2, Iwaoka, Nishi-ku, Kobe, Hyogo 651-24, Japan.

0006-3495/97/10/2012/11 $2.00

MATERIALS AND METHODS

Preparation of kinesin

Bovine kinesin was purified by microtubule affinity purification (Vale et al., 1985) followed by DEAE chromatography and sedimentation. Brains from freshly slaughtered cow (600 g) were homogenized for 20 s in a blender at 4°C with an equal volume of extraction buffer (100 mM MES

(2-(*N*-morpholino)ethane sulfonic acid), 2 mM $MgCl_2$, 2 mM EGTA, 0.1 mM EDTA, 4 mM dithiothreitol (DTT), pH 6.8) including protease inhibitors (0.2 mM PMSF (phenylmethylsulfonyl fluoride), 20 μg/ml leupeptin, 1 μg/ml TAME (nalph-*p*-tosyl-L-argine methyl ester), 2 μg/ml aprotinin, 1 μg/ml pepstatin, 7 μg/ml TPCK (*N*-tosyl-[scp]l-phenylalanine chloromethyl)). The homogenate was centrifuged at 12,000 × *g* for 60 min, and the supernatant was collected and centrifuged at 180,000 × *g* for 60 min at 4°C. To polymerize the endogenous tubulin, GTP (final 0.5 mM) and glycerol (33% v/v) were added to the supernatant and were incubated for 30 min at 33°C. Then 8 units of apyrase (Sigma A-6132) per ml and 40 μM AMP-PNP (5′-adenylylimidodiphosphate) were added to the solution and were incubated for another 10 min at 30°C. The microtubule-kinesin complex was precipitated at 180,000 × *g* for 50 min at 25°C. The supernatant was discarded and the pellet was suspended in 65 ml of buffer 1 (100 mM NaCl, 100 mM PIPES (piperazine-*N,N′*-bis(2-ethanesulfonic acid)), 2 mM $MgCl_2$, 2 mM EGTA, 0.1 mM EDTA, 4 mM DTT, 20 μM taxol, pH 6.8) containing 30% glycerol. The suspension was layered on an equal volume of buffer 1 that contained 50% glycerol and was centrifuged at 180,000 × *g* for 60 min at 25°C. The pellet was suspended in ~20 ml of buffer 1 that contained 10% glycerol. To release the kinesin, 10 mM ATP and 10 mM $MgCl_2$ were added to the suspension, and it was incubated for 20 min at 25°C. The microtubule was precipitated by centrifugation at 190,000 × *g* for 50 min at 20°C. The crude kinesin in the supernatant was loaded onto 0.5 ml of Fractogel EMD in a DEAE column (Cica-MERCK Co.), equilibrated in buffer 2 (20 mM HEPES, 50 mM NaCl, 2 mM $MgCl_2$, 2 mM EGTA, 0.1 mM EDTA, pH 7.5) including 0.2 mM PMSF and 10 μg/ml leupeptin at 4°C. The column was first washed with 5–10 ml of 100 mM NaCl in buffer 2 until the absorbance at 280 nm returned to the baseline, and it was then eluted with 250 mM NaCl in buffer 2. The eluted fraction was enriched with kinesin (2–3 ml) and was further fractionated on a 5–20% (wt/wt) sucrose gradient in A buffer (80 mM PIPES, pH 6.8, 2 mM $MgCl_2$, 1 mM EGTA) containing 0.1 mM EDTA, protease inhibitors, and 1 mM DTT, by centrifugation at 210,000 × *g* for 12 h at 4°C. The protein concentration of the peak kinesin fractions was 0.1–0.2 mg/ml, and the purity was more than 98%. The protein concentration was determined with Coomasie Brilliant Blue staining (Tonein-YP; Ootuka Co., Tokyo, Japan), using bovine serum albumin as a standard. The molar concentration of the kinesin was calculated from the protein concentration of kinesin and the molecular mass of the kinesin at 390 kDa (Kuznetsov et al., 1988). The kinesin was stored in 10-μl aliquots at −80°C after rapid freezing with liquid nitrogen. The entire process took ~35 h.

Preparation of rhodamine-labeled axoneme

Flagellar axonemes were obtained from *Chlamydomonas reinhardtii* by the method of Witman et al. (1978) with some modifications. Axonemes were demembranated with 0.1% Nonidet P40 and were extracted twice with 0.6 M NaCl in a solution (30 mM HEPES, 5 mM $MgSO_4$, 1 mM DTT, 1 mM EGTA) to remove dynein and other accessory proteins (Kagami and Kamiya, 1992). The twice-extracted axonemes were washed once with a HME solution (50 mM HEPES, 2 mM $MgCl_2$, 1 mM EGTA, pH 7.4) and were then suspended in an HME solution. Tetramethylrhodamine succinimidyl ester (C-1171; Molecular Probes, Inc.) (1 μM) was added, and the mixture was incubated at 25°C for 10–30 min. When optimum labeling for the microscopic observation had been achieved, the reaction was halted by the addition of 0.1 M of potassium glutamate. The axonemes were washed twice with a HME solution by centrifugation to remove free rhodamine dye. The final pellet was suspended in an A buffer that contained 50% glycerol and was stored at −20°C.

Bead assays

Kinesin-coated beads were prepared according to the previous methods (Svoboda and Block, 1994a; Higuchi et al., 1997) with some modifications. The A buffer was mixed with filtered casein (final concentration was 1 mg/ml) (AC-solution). Ten percent (v/v) (= 280 pM) fluorescent latex beads (1.0 μm in diameter, carboxylate-modified latex; blue, L5280; Molecular Probes, Inc.) were incubated with the same volume of AC solution for ~20 min on ice. The bead solution (final bead concentration 70 pM) was mixed rapidly with an equal volume of the AC solution that contained kinesin (final concentration 35–685 pM) and was then incubated for another 20 min on ice to make kinesin-coated beads. The fluorescent axonemes were introduced into a flow chamber and were incubated for 3 min to allow tight binding to the chamber surface. The chamber was composed of two coverslips that were separated by 20 μm by two slips of polyethylene film. The two sides of the coverslips were glued with nail enamel. The chamber was washed with an AC solution for 2 min to coat the glass surface with casein and to remove the free axonemes. Finally, the chamber was washed with the A buffer that contained 0.01–1 mM ATP, ~0.04 pM kinesin-coated beads, and photobleaching reducing reagents (10 mM glucose, 9 μg/ml catalase, 50 μg/ml glucose oxidase, 0.5% 2-mercaptoethanol; Harada et al., 1990). All of the procedures were performed at 25–27°C.

Apparatus

The apparatus consisted of a custom-made optical trap microscope and a high-sensitivity detector (Fig. 1) (Higuchi et al., 1997). The device was built on a vibration-free table (1810LA; Hertz) to minimize mechanical vibrations and drift. The stage was moved in a range from 0.1 μm to 2 mm by a hydraulic micromanipulator (WR-3; Narishige) and by a piezo-actuator (NLA 5 × 5 × 9; Tokin). The bead was trapped by a near-infrared laser (Nd:YAG λ = 1064 nm, 300 mW; MYL-300; Santa Fe Laser Co., Santa FE, AZ) through convex and objective lenses (×100, N.A. 1.3; NCF Fluor; Nikon). The fluorescently labeled axonemes and beads were excited by a Green YAG laser (frequency doubled Nd:YAG λ = 532 nm, mode = TEM00, maximum power = 100 mW, rms ripple = 0.2%; model 140-0532-100; Light Wave Electronics) through two convex lenses and a lower objective lens. The epifluorescence images of beads and microtubules were displayed on a TV monitor by a high-sensitivity SIT camera (C-2740; Hamamatsu Photonics). A bright-field image of a trapped bead as illuminated by a green YAG laser was magnified (×1000) and projected onto a quadrant photodiode sensor (size of each pixel, 1.45 mm × 1.45 mm; S994-13; Hamamatsu Photonics) through an upper objective lens (×100, NA 1.25; NCF Plan; Nikon) and a concave lens (*f* = 10 mm). The image of a trapped bead was defocused to enhance the contrast. The displacement of a bead in the *x* and *y* directions was determined by measuring the difference of intensities on each pixel of a quadrant photodiode by using difference amplifiers (OP711A; Sentec, Osaka, Japan).

The stiffness of the kinesin-to-bead linkage was measured during the force generation of the kinesin. To estimate the stiffness, the position of the trapping laser beam was oscillated sinusoidally at amplitude 5 nm (or

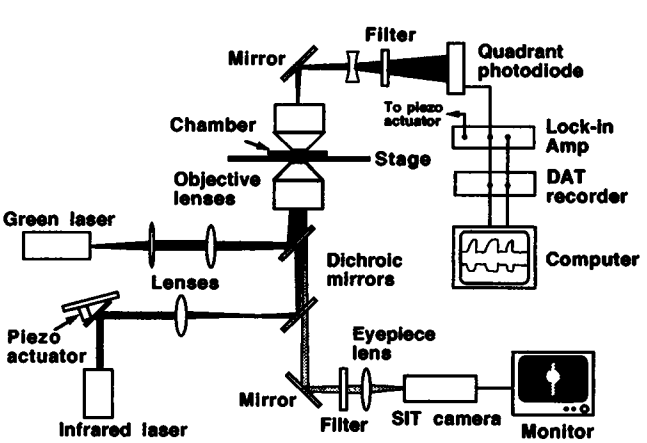

FIGURE 1 Schematic diagram of the laser trapping nanometry system. See text for details.

peak-to-peak amplitude 10 nm) and a frequency of 50–100 Hz by oscillating the angle of a mirror that was mounted on a piezo-actuator (NLA 5 × 5 × 9; Tokin). The amplitude change of the bead oscillation during force generation was detected by using a lock-in amplifier (SR830; Stanford Research Systems). The output signal of the lock-in amplifier is proportional to the amplitude of the sinusoidal oscillation of the bead in a range of 0.5–25 nm. The intercept of the regression line that was fitted to the output signal as a function of amplitude was 0.06 nm, which corresponds to background noise. In our study, background noise of 0.06 nm was not taken into account, because the amplitude during force measurement was >1 nm.

Data were recorded with a DAT recorder (RD-120TE; TEAC) at a sampling rate of 24 kHz per channel. Data were also collected at low temporal resolution, at a sample rate of 200-1000 Hz, with a computer (Macintosh PC7100, Apple) that was equipped with a laboratory interface board (MacLab, ADInstruments). Before digital sampling, the signal was filtered through a low-pass filter at a cutoff frequency that was half that of the applied sinusoidal oscillation. The time constant of the bead position sensor was 0.016 ms (feedback resistor = 1 MΩ). Spectral analyses were performed with waveform analysis software (DADisp, Astro design). To extract the stepwise motion from the noise, some of the data that had been recorded with the MacLab and the DAT recorder were passed through a median filter with 15-ms windows. This is a nonlinear filter that removes high-frequency noise while preserving edge information.

The bead displacement was calibrated as follows. The magnification of a bead's image at the detector plane was precisely adjusted to ×1000, using the image of a stage micrometer that had been projected on the detector as a standard. The image of a bead was projected onto the detector, and the detector was moved sinusoidally in the directions of x and y at a frequency of 20 Hz and an amplitude of 5 μm by a piezo-actuator. The displacement of a bead's image projected onto the detector (5 μm) corresponds to 5 nm of the bead displacement at the sample plane.

RESULTS

Noise and calibration of nanometry

A latex bead, 1 μm in diameter, was fixed to the surface of a flow chamber and was moved by using a piezo-actuator that was mounted to a stage (Fig. 1). The noise on the differential output of the quadrant detector during single movement of stage was 0.33 nm in SD (Fig. 2 *a*, *lower trace*). The output of the detector averaged for four beads was proportional to the displacements of a bead at < ~150 nm but deviated slightly from linear relationships at > ~200 nm (Fig. 2 *b*). We calibrated the detector by using the relationship between the displacements of a bead and the differential output that was obtained for each bead that was used in the experiments.

The stiffness of the optical trap (K) was determined from the variance of the thermal fluctuations of a trapped bead that was based on the Equipartition Theorem: $K\langle x^2\rangle = k_bT$, where k_b is the Boltzmann's constant (1.38×10^{-23} J/K), T is the absolute temperature (298 K), and x is the displacement of the bead from the trap's center. Variance ($\langle x^2\rangle$) was obtained by integrating the power spectrum density (PSD) of the thermal fluctuations of the bead that were captured in an optical trap (Fig. 2 *d*). The power density spectra showed a Lorentzian curve that was given as $PSD = A/(1 + (f/f_c)^2)$, where A is the power density at zero Hz, f is the frequency, and f_c is the corner frequency. The integral of this spectrum can be given by $\pi A f_c/2$ ($= \langle x^2\rangle$), and K was calculated as $K = 2k_bT/(\pi A f_c)$. The noise from the bead that was fixed on a flow chamber and from the bead that was trapped by a YAG laser (K = 0.26 pN/nm) is shown in Fig. 2 *c*. Stepwise movement of more than 1 nm was not observed in either trace. By the analysis of the power density spectrum, system noise, which came from a green YAG laser and the mechanical and thermal vibrations of the apparatus, was <0.1 $nm/Hz^{0.5}$ in a frequency range of >1 Hz (Fig. 2 *d*). Total noise without a bead was ~0.2 nm at 0.5 Hz to 10 kHz, which was obtained by integrating the power density spectrum of light noise in Fig. 2 *d*. Trap stiffness, K, increased linearly with an increase in the laser power (Fig. 2 *e*). Next we examined the possibility that trap stiffness might be affected by some unknown interactions with the glass surface. However, stiffness was unchanged when the gap between the bottom surface of the bead and the glass surface varied from <0.1 to 5 μm. In general, we measured the thermal fluctuations of the bead at a gap of 2 μm to determine trap stiffness.

The trap stiffness at a wide range was determined by measuring the displacement of a bead that was caused by the solution flow (Svoboda and Block, 1994b). The viscous drag on the bead at a flow rate of v was calculated as γv, where γ is the viscosity coefficient. γ was determined from the relationship of $\gamma = K/(2\pi f_c)$, using the K and f_c values that were calculated from thermal fluctuations. Fig. 2 *f* shows the relationship between the drag forces and the displacements of the bead at various laser power levels. The displacements increased linearly in a range of ±300 nm with an increase in the flow rate.

The number of kinesin molecules bound to a bead

The number of kinesin molecules on a bead that can interact with a microtubule was estimated by the statistical method of Svoboda and Block (1994a). Fig. 3 shows the probability that the bead moved upon being placed contact with an axoneme at various number ratios of kinesins to beads in the mixing solution. The data fit an exponential curve that is given by $1 - \exp(-n/1.9)$, where n is the number ratio of kinesins to beads at mixing. When the molar ratio of the kinesin molecule to the bead was 1.9, the average number of functional kinesin molecules that were absorbed on a bead is 1. This indicates that the distribution of kinesin molecules on the beads follows Poisson statistics. The probability was unchanged when the incubation time of beads and kinesins was changed from 20 min to 10 h. The experiments were performed with a probability of 0.41, i.e., a number ratio of mixing kinesins and beads of 1. Under these conditions, the probability of the bead adsorbing more than two kinesins can be given by the equation $1 - \exp(-1/1.9) - (1/1.9)\exp(-1/1.9) = 0.10$ (Svoboda and Block, 1994a). Taking the geometry of the kinesin on the bead into account (Svoboda and Block, 1994a), the probability that only single kinesin molecules interacted with an axoneme is >99%.

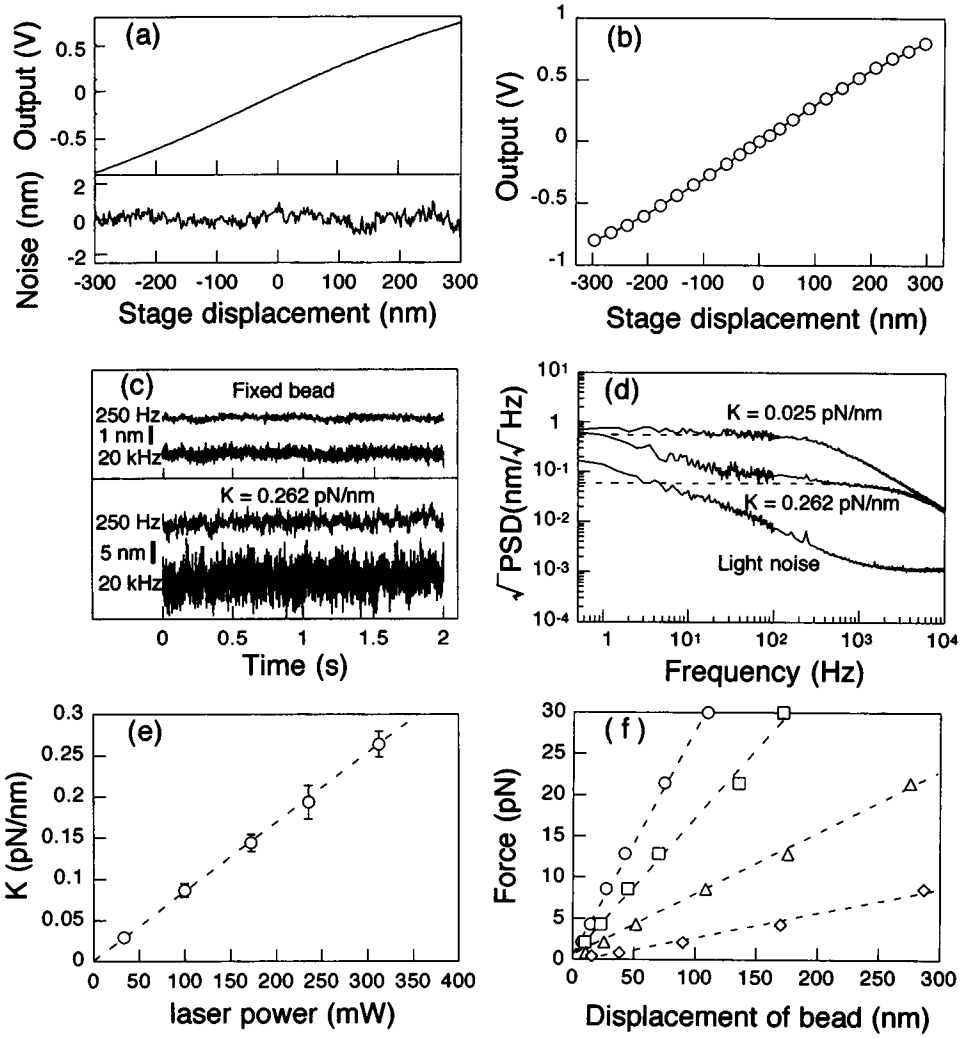

FIGURE 2 Calibration of the apparatus. (*a* and *b*) Response curve of the quadrant photodiode. A latex bead fixed on a coverslip was moved by a piezo actuator. (*a*) *Upper trace*: Photodiode output in response to the constant velocity movement of a coverslip. Data were filtered by a 250-Hz low pass filter. *Lower trace*: The fluctuation of the photodiode output. The upper trace was fitted by a fifth-order polynomial, and the difference between the fitting curve and the upper trace was calculated. (*b*) The beads were vibrated sinusoidally with amplitudes of 10–300 nm. The amplitudes of displacement of the piezo-actuator are proportional to those of input voltages applied, although the overall movement of the piezo-actuator shows hysteresis to input voltage. The average of photodiode output was plotted as a function of the displacement of the bead from the center of the trap. (*c*) Noise of a bead that had been fixed on a coverslip (*upper traces*) or a bead trapped by a YAG laser (*lower traces*). The noise signal was filtered by 250-Hz and 20-kHz low-pass filters. (*d*) Square root of the power spectrum density of the bead fluctuation and apparatus noise. *Upper and middle traces*: Bead fluctuations. Spectra at frequencies of >100 Hz were fitted by a Lorentzian curve that is shown by the dotted line. *Upper trace*: The corner frequency of the spectrum was 333 Hz, and trap stiffness was calculated as 0.025 pN/nm from the equipartition theorem. *Middle trace*: The corner frequency was 2870 Hz and the trap stiffness was 0.262 pN/nm. *Lower trace*: Light noise of the green YAG laser. (*e*) Trap stiffness as a function of laser power. Trap stiffness was calculated by the equipartition theorem (see text for details). Laser power was measured at the position of the piezo actuator, which is shown in Fig. 1. The power at the sample plane was reduced to ~30% of that at the piezo position by mirrors and an objective lens. (*f*) Relation between the bead movements and the viscous drag force at various levels of laser power.

Displacements and forces

The displacements and forces that are caused by single kinesin molecules were measured at a trap stiffness of 0.025–0.30 pN/nm at 10 μM (Fig. 4 *a*, *upper trace*) and 1 mM ATP (Fig. 7 *a*). When the bead was placed in contact with an axoneme, the bead was rapidly displaced from the trapping center and then gradually decreased its displacement velocity until it reached a plateau. The bead stayed at almost constant plateau levels for a given period of time and then returned to the trap center. On some occasions, the bead returned to the trap center before reaching the plateau (Fig. 4 *a*). We measured the stall force in which beads stay for a period that is longer than 0.2 s at 1 mM ATP and 0.5 s at 10 μM ATP. The stall forces were independent of the ATP concentrations, 7.2 ± 1.3 pN (mean ± SD, n = 132) at 1 mM ATP and 7.4 ± 1.4 pN (n = 57) at 10 μM ATP. The stall forces were also independent of trap stiffness in a range of 0.025–0.30 pN/nm.

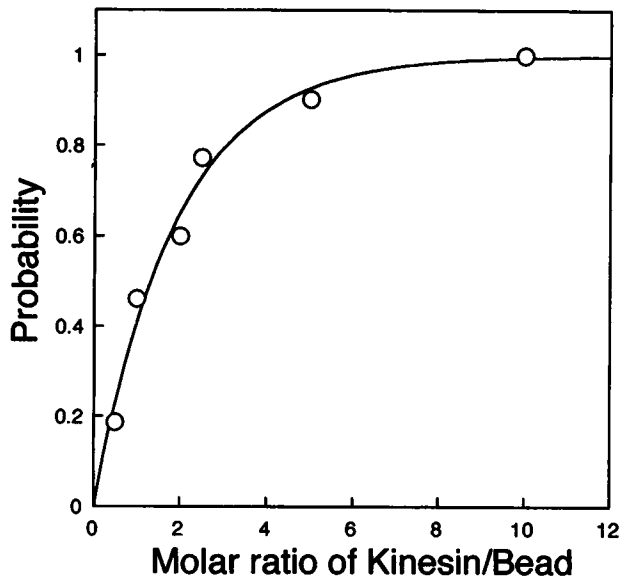

FIGURE 3 Probability of a moving bead at various molar ratios of kinesin to bead at mixing. The beads were brought into contact with an axoneme three times for 30 s. The probability of the kinesin bead moving onto the axoneme was measured. The number of beads that were measured at each point was 7–22 and the total number was 99. The solid line is the fitted curve as $1 - \exp(-x/1.9)$, where x is the molar ratio of kinesin to bead.

Force-velocity relation

A lower trace in Fig. 4 *a* shows the amplitude of sinusoidal change of a bead position when the position of trap center changed sinusoidally. The displacement caused by the kinesin was calculated from bead displacement and the amplitude of sinusoidal bead movement. By averaging the 17 traces of force and amplitude at 10 μM ATP, the traces in Fig. 4 *a* were smoothed out (Fig. 5, *a* and *b*). The kinesin displacement (ΔX_k) relative to a microtubule is given as $\Delta X_k = \Delta X_b + \Delta X_p$, where ΔX_b is the bead displacement and ΔX_p is the total longitudinal extension of the linkages between bead and kinesin, kinesin and axoneme, and axoneme and glass (Fig. 4 *b*, *bottom diagram*; Ishijima et al., 1991; Svoboda and Block, 1994a). Because the trapping force ($K \cdot \Delta X_b$) is balanced by the extension force ($K_p \cdot \Delta X_p$) of the linkages (Fig. 4 *b*, *bottom diagram*), ΔX_k is calculated as $(1 + K/K_p) \cdot \Delta X_b$, where K_p is the linkage stiffness. K was obtained as described above. K_p was estimated from the amplitude (ΔX) of the bead displacement when the laser beam was sinusoidally oscillated with an amplitude of 5 nm (ΔX_t) during force generation (Fig. 4 *b*, *middle diagram*). From the force balance between the extension force of the linkage ($K_p \cdot \Delta X$) and the trap force ($K \cdot (\Delta X_t - \Delta X)$), K_p can be calculated as $K \cdot (\Delta X_t - \Delta X)/\Delta X$ (Fig. 5 *c*). Kinesin displacement (ΔX_k) was calculated as $\Delta X_k = \Delta X_b \cdot \Delta X_t/(\Delta X_t - \Delta X)$, where $\Delta X_t/(\Delta X_t - \Delta X)$ is an attenuation factor (Fig. 5 *d*) for calculating the kinesin displacement from the bead displacement. To obtain the total kinesin displacement, we integrated ΔX_k (Fig. 5 *e*).

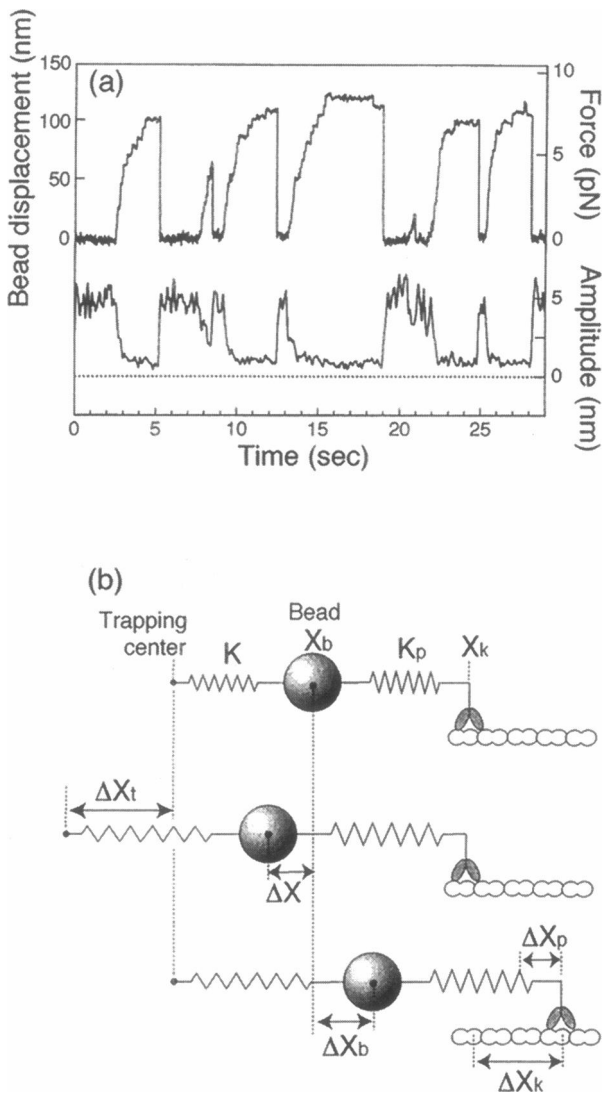

FIGURE 4 Movement of the bead and the stiffness measurement of the linkage between the kinesin and microtubule. (*a*) *Upper trace*: Displacement of the kinesin-coated bead interacting with an axoneme at an ATP concentration of 10 μM. Force (*right upper scale*) of kinesin was calculated from the displacement of a bead that was multiplied by the trap stiffness: 0.070 pN/nm. *Lower trace*: Amplitude of the sinusoidal movement of the bead as detected by a lock-in amp. The trap center was sinusoidally oscillated at 100 Hz at an amplitude of 5 nm. The displacement signal of the kinesin and the amplitude were filtered by 25-Hz and 5-Hz low-pass filters, respectively. (*b*) Mechanical model for the displacement of a kinesin and a bead. See text for details.

The amplitude of the sinusoidally oscillated beads (ΔX) decreased with force (Figs. 4 and 5 *b*), indicating that the linkage stiffness K_p depends on the force (Fig. 5 *c*). The amplitude returned to its original value when the bead was dissociated from a microtubule. The K_p value at the plateau force level (6–8 pN) was 0.34 ± 0.08 pN/nm (mean ± SD, $n = 60$), which was independent of the trap stiffness in a range of 0.025–0.30 pN/nm. The application of sinusoidal oscillations to the bead did not affect the movement and force of a kinesin, i.e., the slope of the displacement and the

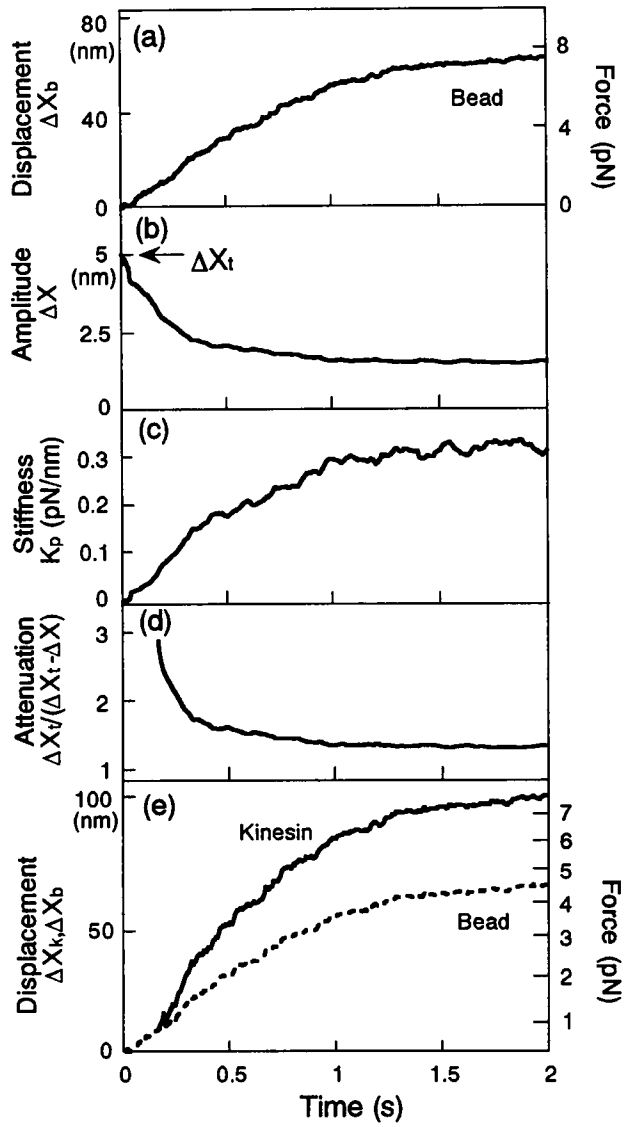

FIGURE 5 The average displacement of kinesin as estimated from bead displacement and linkage stiffness between the bead and the proteins. (*a*) Seventeen traces of displacement (ΔX_b) of beads, in which kinesin molecules did not detach for >2 s, were averaged. The force was calculated from the displacement of the bead times the trap stiffness. The displacement signals were filtered with a 50-Hz low-pass filter. ATP: 10 μM; trap stiffness (K): 0.12 pN/nm. (*b*) Amplitude (ΔX) of a bead when the trap center was sinusoidally oscillated at 100 Hz at an amplitude of 5 nm (ΔX_t). The amplitude was simultaneously determined with a displacement measurement, shown in *a*. (*c*) The stiffness (K_p) of the linkage was calculated from the amplitude shown in *b*. The stiffness was given by $K(\Delta X_t - \Delta X)/\Delta X$. (*d*) The attenuation factor as calculated from the amplitude as shown in *b*. The attenuation factor is given by $\Delta X_t/(\Delta X_t - \Delta X)$. Attenuation factors greater than 3 were deleted because of the large amount of noise. (*e*) Solid line: The total displacement of kinesin was given by integrating the kinesin displacement, which was calculated by attenuation factor (*d*) as multiplied by the bead displacement (*a*) for a 60-ms period. Kinesin displacement was calculated at a force of >1 pN to avoid a large amount of noise in the attenuation factor at low force.

stall force. Data analysis for the force-velocity relation curve was performed only for values greater than 0.5 pN because of the large amount of noise at values less than 0.5 pN. The relationship between force and velocity (Fig. 6) was obtained from the averaged displacement traces, as shown in Fig. 5 *e*. The velocities at zero force were measured from a video image of the beads when the kinesin beads were released from an optical trap. Velocity at 10 μM ATP was about one-third of that at 1 mM ATP at zero load. At both ATP concentrations the kinesin velocity decreased almost linearly with an increase in force (Fig. 6).

Step size

The step movements of beads could be clearly observed at higher forces greater than 3 pN (Figs. 4 *a* and 7), because the stiffness of the kinesin-bead linkage was large enough to distinguish the step movement from the thermal noise. To determine whether the size of the kinesin step was independent of the velocity, we analyzed the step size at ATP concentrations of 10 μM and 1 mM, at medium and high loads. The observed step sizes were mostly ~ 8 nm and ~16 nm at the low time resolution (50-Hz low-pass filter) (Fig. 7). Sixteen-nanometer steps are made up of two sequential ~8-nm steps at higher time resolution (250-Hz low-pass filter) (Fig. 7 *d*, *inset*). Fig. 8 shows histograms of net kinesin displacements within window sizes of 50 ms (Fig. 8 *a*), 100 ms (Fig. 8, *b–d*), or 10 ms (Fig. 8, *e* and *f*) during force generation. The histograms were fitted to multiple Gaussians that were centered at approximately −8, 0, 8, 16, 24, 32, and 40 nm. The Gaussian distributions are thought to be due primarily to the randomizing effects of thermal noise of the bead. The center of each Gaussian was

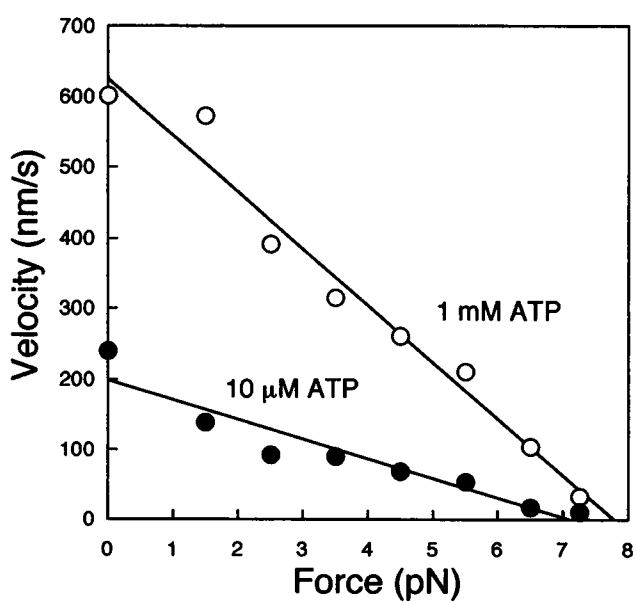

FIGURE 6 Force-velocity relations. Velocities were calculated from the slope of the kinesin displacement curve (Fig. 5 *e*). ○, 1 mM ATP; ●, 10 μM ATP. The velocities at zero pN were measured without a trapping laser. Each of the data points represents the average value in the range of 1–2, 2–3, 3–4, 4–5, 5–6, 6–7, and 7–7.5 pN.

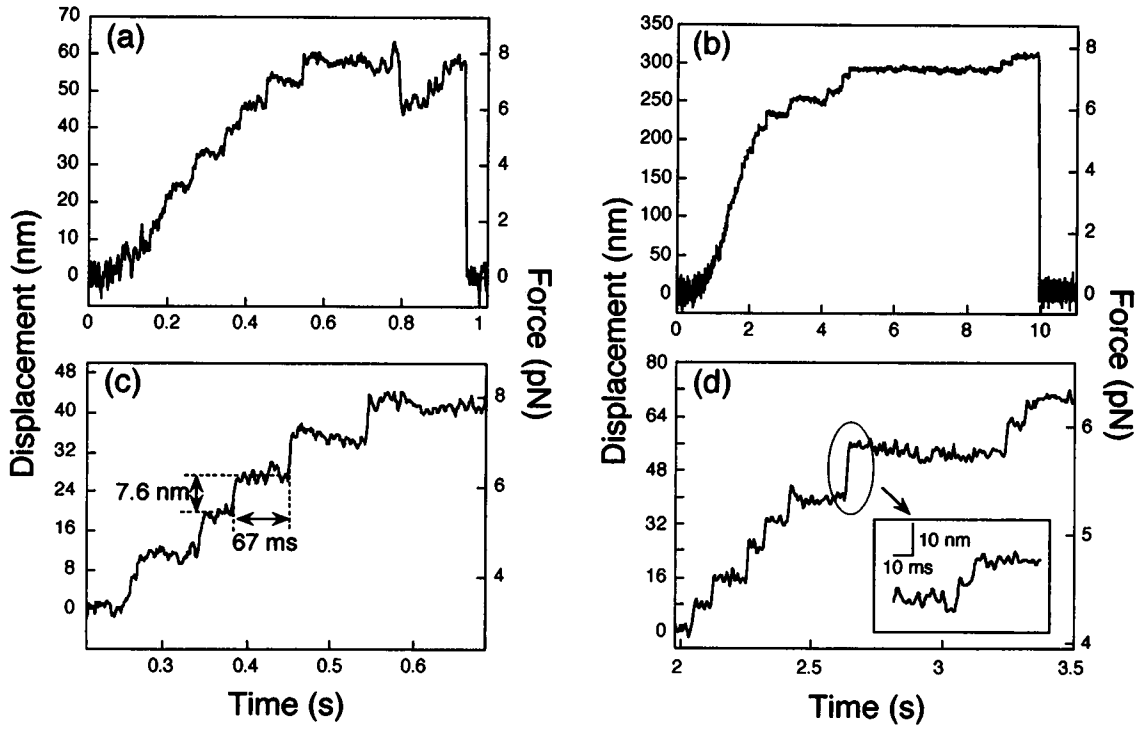

FIGURE 7 Stepwise movements of beads at 1 mM ATP (*a*) and 10 μM ATP (*b*). In *c* and *d*, displacements that express kinesin movement are corrected from *a* and *b*, respectively, by using the attenuation factor as shown in Fig. 5 *e*. The force was calculated from the trap stiffness and bead displacement. Trap stiffness: (*a*) 0.13 pN/nm; (*b*) 0.025 pN/nm. Filters used in the displacement: (*a* and *c*) 100-Hz low-pass filter; (*b* and *d*) 50-Hz low-pass filter. (*d, inset*) 250-Hz low-pass filter. The step size, shown in figures, was measured from the differences in the averages of the displacements between the steps. The time in *c* indicates the dwell time. Dwell time was measured between steps when displacements were half of the unitary steps.

a multiple of ~8 nm and was independent of the load and the ATP concentrations. At both low and high loads (Fig. 8, *d* and *f*), the size of most of the steps was ~8 nm. We did not observe any 3–6-nm steps in Fig. 8. These results indicate that the unit step size is ~8 nm, and step sizes that are longer than 16 nm are due to multiple unitary 8-nm steps but not to single 16-nm steps. Backward steps 8 nm in size were occasionally observed as well at time resolution of 10 ms. The number of backward steps was 2–8% that of the forward steps at 3–6-pN forces and increased slightly to ~10% near the stall force (6–8 pN).

Dwell time

To examine the kinetics of step reaction, the dwell times (Fig. 7 *c*) between adjacent 8-nm steps were measured at 1 mM and 10 μM ATP and at 3–6 pN (Fig. 9). Data were analyzed at a temporal resolution of 2 ms to distinguish the 8-nm steps. The time necessary to generate an 8-nm step was determined as the time at the center of the 8-nm steps (Fig. 7 *c*). At high and low ATP concentrations, dwell-time distributions show a monotonic decrease (Fig. 9). To explain this, it is important to take into account the fact that a kinesin molecule has two heads, as will be discussed later.

DISCUSSION

Improvement of the nanometry system

To accurately measure stepwise movements, a large signal-to-noise ratio for the detection of bead displacement is essential. We have shown previously that the noise due to photodiodes and electric circuits at >10 Hz can be reduced by ~10 times by replacing the halogen lamp that is used to illuminate the bead with an intense green semiconductor laser with a light intensity that is ~100 times larger (Ishijima et al., 1996). However, the noise at low frequencies of <10 Hz was still large. Low-frequency noise results from flickering of the interference pattern that is produced by the illuminating green laser. These interference patterns were minimized by reducing the number of external lenses to three, because most lenses produced prominent interference patterns. As a result, the interference pattern was almost eliminated and light noise at a low frequency of 1 Hz was reduced to ~0.1 nm/$Hz^{0.5}$ (Fig. 2 *d*), which was less than half of the noise that was observed with a halogen lamp. Furthermore, no artifactual step was observed in the measurement of the signal from the bead that had been fixed on a glass surface (Fig. 2 *c*). Another advantage of using a green semiconductor laser is that it produces little heat and therefore less noise at low frequency. As shown in Fig. 4 *a*, the thermal drift of the displacement baseline was negligible

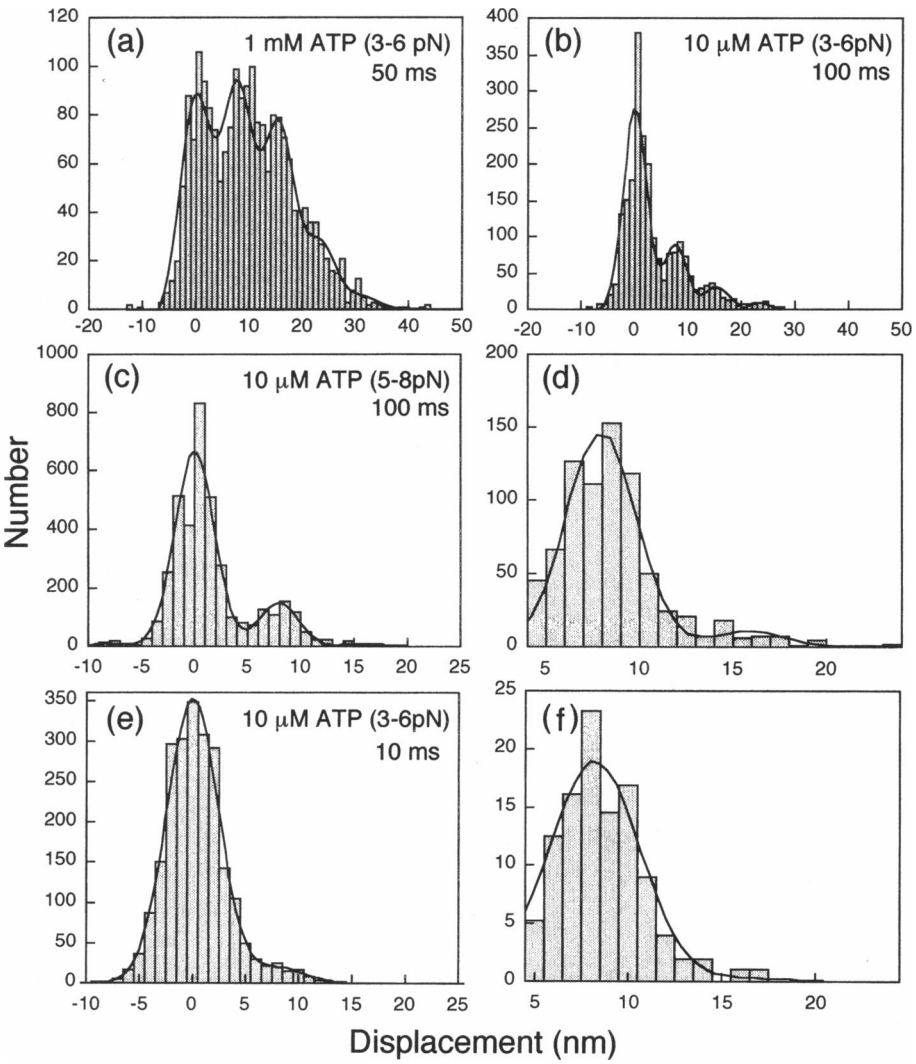

FIGURE 8 Histograms of step size. Duration window of 50 ms (*a*), 100 ms (*b–d*), or 10 ms (*e* and *f*) was moved every 5 ms, and, for each of those windows, we measured the net displacement in a given period. (*a*) 1 mM ATP and force of 3–6 pN; (*b*, *e*, and *f*) 10 μM ATP and 3–6 pN; (*c* and *d*) 10 μM ATP and 5–8 pN load. Number of measured force traces, 14–60. Histograms were fitted by the least-squares method, with the multiple of step size with a Gaussian distribution as indicated by the following equation: summation of i = −1 to 5 of $Ai \cdot \exp\{-(x - i \cdot D)^2/(2\sigma^2)\}$, where D is the elementary step size, and Ai and σ are the amplitude and the standard deviation of the Gaussian distribution, respectively. D and σ were 7.8 and 2.9 nm (*a*), 7.7 and 2.2 nm (*b*), 7.9 and 1.9 nm (*c*), and 8.2 and 2.5 nm (*e*), respectively. (*d* and *f*) Gaussian distribution at ~0 nm was subtracted from *c* and *e*, respectively.

for 30 s. The rate of the drift of the baseline was only 1–10 nm/min. Thus we could accurately measure the bead displacements over a wide frequency range.

Stiffness measurement

The step size of the kinesin molecules was calculated from the displacement of the kinesin-coated beads and the stiffness of kinesin-to-bead linkage. Simultaneous measurement of the force and stiffness is essential to accurately determine step size. Stiffness can be measured from the mean square value of the thermal motion of the bead (Svoboda and Block, 1994a), if kinesin does not generate step movements and the low-frequency system noise is negligible. This, however, is not the case. Therefore, in this study the stiffness of the linkage between the kinesin molecules and the beads was detected by the sinusoidal response of the bead by using a lock-in amplifier to determine the linkage stiffness.

We used axonemes instead of microtubules because the linkage stiffness of bead-kinesin-axoneme was 0.34 pN/nm at 6–8-pN load, which was more than two times larger than that of the bead-kinesin-microtubule (Svoboda et al., 1993; Higuchi et al., 1997). This is probably due to the rigid binding of the axoneme to the glass surface. The mean square value of the thermal noise of a bead is proportional to the inverse of linkage stiffness + trap stiffness. Therefore, as linkage stiffness increases, thermal noise decreases. Stepwise kinesin movements can be more easily and more clearly detected with axonemes as compared with microtubules (Fig. 7).

Linkage stiffness increased with an increase in force (Fig. 5 *c*). This nonlinear elasticity may come from the nonlinear elasticity of the kinesin or the microtubule and/or nonlinear elasticity due to the rotation of the bead (Dupuis et al., 1997). Despite the linkage that exhibited nonlinear elasticity, it is possible to estimate accurately the displacement of the kinesin when the displacement of kinesin and linkage stiffness are measured simultaneously.

Stall force

The stall forces of single kinesin molecules were 7.2–7.4 pN at 10 μM and 1 mM ATP. The stall forces were determined

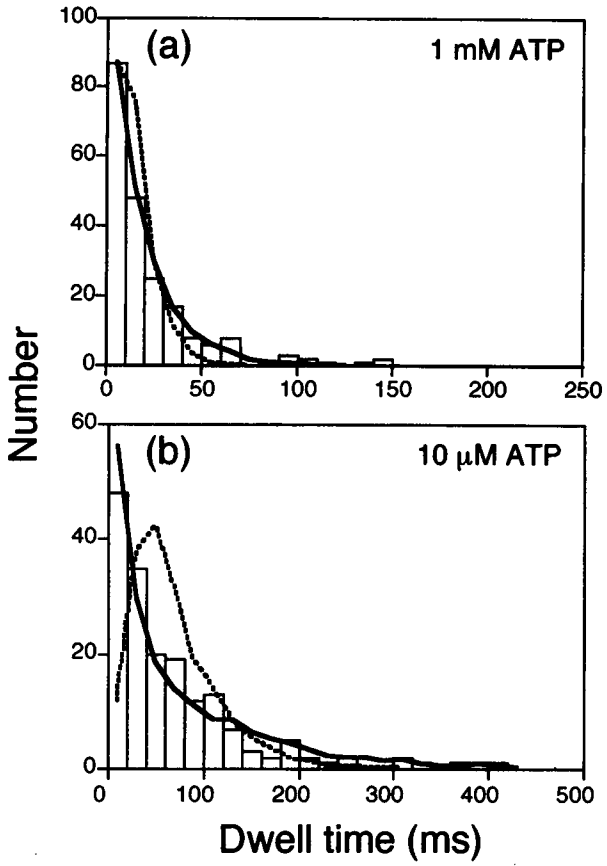

FIGURE 9 Histograms of the dwell time of the steps. (*a*) 1 mM ATP and 3–4 pN; (*b*) 10 μM ATP and 3–4 pN. Widths of data bin are 10 ms (*a*) and 20 ms (*b*). Solid lines are the best fitted curves that were obtained by the least-squares method by simulating a 16-nm stepping model (Fig. 10 *a*) at t_b of 19 ms and t_a of 1 ms (*a*), t_b of 19 ms and t_a of 100 ms (*b*). Both t_a and t_b were changed to obtain the best fitted curves. t_a and t_b are transition time averages, which were exponentially distributed with probabilities of $\exp(-t/t_a)$ and $\exp(-t/t_b)$, respectively. Simulation was done via a Macintosh PC7100 with LabView Ver 3.1 software (National Instruments Co.). The curves were obtained by simulating the position of the kinesin heads for 100,000–300,000 iterations, with a time resolution of 1 ms. Broken lines are the best fitted curve (least mean-square method) that were obtained by simulating only an 8-nm step occurrence (Fig. 10 *b*) at t_b of 9.5 ms and t_a of 1 ms (*a*), t_b of 9.5 ms and t_a of 50 ms (*b*).

by measuring the plateau forces, which remained constant for periods of more than 0.2 s at 1 mM ATP and 0.5 s at 10 μM ATP. This value was close to that obtained previously (6.7 pN; Higuchi et al., 1997) but slightly larger than those reported previously (5–6 pN, Svoboda et al., 1993; ~5 pN, Meyhoefer and Howard, 1995). The differences may be due to the fact that previous studies may have measured the forces before they reached the plateau. Because the force increased very slowly near the plateau, determining the true value was not easy. The true stall force is not larger than 10 pN, because no force of >10 pN has been observed to date.

Force-velocity relation

The force-velocity relationship was linear in the whole range from zero to the maximum force (Fig. 6). Similar linear force-velocity curves have previously been reported (Svoboda and Block, 1994a; Meyhoefer and Howard, 1995); however, the relationship near the zero force and zero velocity was not clear, because the stiffness of the linkage had not been estimated. The linear relationship between the force and the velocity of the kinesin-microtubule motor is different from that of skeletal muscle, where the force-velocity curve is hyperbolic when measured under isotonic conditions and slightly convex under auxotonic ones. This difference may be due to the difference in the character of the kinesin-microtubule motor and that of an actomyosin motor. It may also be due to the fact that the force-velocity relationship for single myosin molecules is modulated in muscle, because a huge number of actomyosin motors operate together in muscle.

Unitary step size

We observed 8-nm steps and steps in multiples of 8 nm in kinesin-coated beads under 3–8-pN load at a low time resolution (50–100 ms in Fig. 8) as previously reported (Svoboda et al., 1993; Higuchi et al., 1997; Inoue et al., 1997). Measurements at high time resolution showed that the large steps were due to sequential multiples of 8-nm steps (Fig. 7 and 8), which occurred within 50–100 ms. The peak of the 3–6-nm steps could not be observed in Fig. 8. Therefore, the unitary step size of kinesin-coated beads under a 3–8-pN load is most likely 8 nm (Fig. 8, *d* and *f*).

There is still the question of how the individual heads of a two-headed kinesin molecule step on microtubules. A kinesin molecule consists of two heavy chains, each of which contains a motor domain that forms a ~7-nm globular head (Kull et al., 1996), a short neck region, a long coiled coil structure that dimerizes the two heavy chains, and a C-terminal globular domain that binds a light chain (Huang et al., 1994). Electron microscopy showed that a kinesin head binds with an 8-nm periodicity to β-tubulin in microtubules (Song and Mandelkow, 1993). The stride between the forward and the rear heads must be restricted by the length of the neck domains (Huang et al., 1994). Therefore, the heads of a kinesin molecule could not bind to β-tubulins that are 16 nm or more apart at the same time. Correspondingly, we barely observed step sizes of 16 nm and longer at high time resolution or low velocity (Fig. 8, *d* and *f*). Thus two possible models of the 8-nm step of a kinesin molecule are shown in Fig. 10, *a* and *b* (Block and Svoboda, 1995). We have assumed that the position of the kinesin-coated beads is determined by the position of the forward head because the forward head must be loaded. In the model in Fig. 10 *a*, the two heads of a kinesin molecule move along the same or adjacent protofilaments and step ~16 nm in a hand-over-hand manner (16-nm stepping model). In the model in Fig. 10 *b*, the two heads of a kinesin molecule step ~8 nm along the adjacent protofilaments (8-nm stepping model). If the position of kinesin-coated beads in the 8-nm stepping model is determined by the

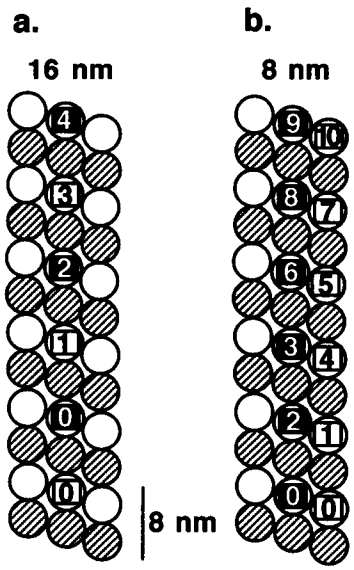

FIGURE 10 Kinesin stepping models. *Open circles*, β-tubulin. *Hatched circles*, α-tubulin. *Open and closed squares*, kinesin heads. *Numbers in squares*, order of steps. (*a*) 16-nm stepping model. In this model, the movements of the kinesin molecules that were caused by a single step of a head are ~8 nm. (*b*) 8-nm stepping model. In this model, the movements of kinesin molecules that were caused by a single step of a head varied from ~1 nm (first to second step), ~8 (second to third step), ~0 (third to fourth step), and ~7 (fourth to fifth step).

average position of two heads, only the 4-nm step should be observed. The fact that the step size of kinesin-coated beads was 8 nm excludes this possibility and supports the assumption that the position of a forward head determines the position of the kinesin-coated beads. The possible kinesin displacements that are caused by head movements are the 8, 7, 1, and 0 nm in the 8-nm stepping model and 7, 8, and 9 nm in the 16-nm stepping model, because the tubulins in the adjacent protofilaments shifted by ~1 nm (Fig. 10). A small variety in step sizes (~1 nm) could not be detected with the present measurement, however, because of the thermal fluctuation of the beads. Both the 8-nm and 16-nm stepping models assume that at least one head of a kinesin molecule always binds to a microtubule to prevent the dissociation of the bead from a microtubule.

Step model deduced from dwell time

To determine which of the 8-nm or 16-nm stepping models best fit the experimental data, the histograms of the dwell times (Fig. 9, *a* and *b*) were simulated with the following simplified kinetic model:

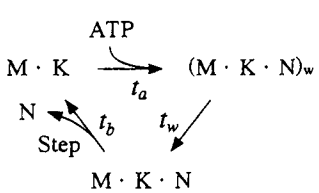

where K is a kinesin head, M is a microtubule, N is a nucleotide (ATP, ADP · P_i, or ADP) and $(\ldots\ldots)_w$ means the "waiting state." t_a and t_b are the transition times (inverse of the rate). t_a depends on the ATP concentration but t_b does not. Because the heads could not bind to β-tubulins that were separated by 16 nm or more at the same time, we assumed that when a forward head with nucleotide is separated by ~8 nm from a rear head, the forward head pauses for a waiting time t_w at the $(M \cdot K \cdot N)_w$ state until the rear head steps and transfers to the M · K · N state just after the rear head steps. To simplify the model, we have assumed that kinesin heads act in an equivalent manner, and t_a and t_b are independent of the heads' positions. As for the 16-nm stepping model, the forward head goes through the M · K, $(M \cdot K \cdot N)_w$, and M · K · N states and the rear head skips the $(M \cdot K \cdot N)_w$ state. As for the 8-nm stepping model, the forward head with nucleotide pauses at the $(M \cdot K \cdot N)_w$ state when the forward head is separated by ~8 nm from the rear head but does not pause when the forward head is close (0–1 nm) to the rear head. The rear head skips the $(M \cdot K \cdot N)_w$ state.

The parameters t_a and t_b were determined by fitting the stochastically simulated curves to the dwell-time histograms. Our simulation (Fig. 9) showed that both of the dwell-time histograms at high and low ATP concentrations were adequately explained by the 16-nm stepping model. Simulation based on the 8-nm stepping model could not fit the histogram of dwell time at low ATP concentration (Fig. 9 *b*). Therefore we have concluded that kinesin heads primarily step by 16-nm steps in a hand-over-hand manner. The values of t_a and t_b that produced the best curve fits were 1 and 19 ms, respectively, at 1 mM ATP, and 100 and 19 ms, respectively, at 10 μM ATP. The average cycle times were 38 ms at 1 mM ATP and 159 ms at 10 μM ATP. The waiting time t_w was calculated from the average cycle time minus $(t_a + t_b)$: 38 − (1 + 19) = 18 ms at 1 mM ATP and 159 − (100 + 19) = 40 ms at 10 μM ATP. The waiting time was 47% and 25% of the cycle times at 1 mM and 10 μM ATP, respectively. The waiting state is, therefore, an important state in the ATPase reaction of the kinesin-microtubule complex.

The 8-nm stepping model was ruled out on the assumption that t_a and t_b are independent of the positions of heads. However, t_a and t_b may depend on the relative positions of the two heads. If the heads step cooperatively, the dwell-time histograms may be explained by the 8-nm stepping model as well.

Recently the three-dimensional structure of kinesins and a microtubule complex that had been reconstructed from the electron micrograph showed that one head of kinesin binds to a microtubule (Hirose et al., 1996). Based on these results, Hirose and co-workers proposed a 16-nm step hand-over-hand model. Their model is consistent with ours. In the 16-nm step hand-over-hand model simulation, the value obtained for t_a was 100 ms at 10 μM ATP, i.e., the second-order rate constant of ATP binding was calculated to be 10^6 M^{-1} s^{-1} and t_b was 19 ms. Recently Higuchi and colleagues

(1997) determined the rate constants for ATP binding to the microtubule-kinesin complex and force generation under conditions similar to ours. They found that the second-order rate constant of ATP binding was $\sim 0.7 \times 10^6\ M^{-1}\ s^{-1}$ and the time for entry into the force-generating state for kinesin was ~20 ms. These values are consistent with the present t_a and t_b values. These support the conclusion that the kinesin heads step by 16 nm, whereas the kinesin-coated beads move by 8-nm steps.

We thank Drs. Robert A. Cross and Jan West for helpful discussions.

REFERENCES

Block, S. M., and K. Svoboda. 1995. Analysis of high resolution recordings of motor movement. *Biophys. J.* 68:230s–241s.

Coppin, C. M., J. T. Finer, J. A. Spudich, and R. D. Vale. 1996. Detection of sub-8-nm movements of kinesin by high-resolution optical-trap microscopy. *Proc. Natl. Acad. Sci. USA.* 93:1913–1917.

Dupuis, D. E., W. H. Guilford, J. Wu, and D. M. Warshaw. 1997. Actin filament mechanics in the laser trap. *J. Muscle Res. Cell Motil.* 18: 17–30.

Finer, J. T., R. M. Simmons, and J. A. Spudich. 1994. Single myosin molecule mechanics: piconewton forces and nanometre steps. *Nature.* 368:113–119.

Funatsu, T., Y. Harada, M. Tokunaga, K. Saito, and T. Yanagida. 1995. Imaging of single fluorescent molecules and individual ATP turnovers by single myosin molecules in aqueous solution. *Nature.* 374:555–559.

Harada, Y., K. Sakurada, T. Aoki, D. D. Thomas, and T. Yanagida. 1990. Mechanochemical coupling in actomyosin energy transduction studied by in vitro movement assay. *J. Mol. Biol.* 216:49–68.

Higuchi, H., E. Muto, Y. Inoue, and T. Yanagida. 1997. Kinetics of force generation by single kinesin molecules activated by laser photolysis of caged ATP. *Proc. Natl. Acad. Sci. USA.* 94:4395–4400.

Hirose, K., A. Lockhart, R. A. Cross, and L. A. Amos. 1996. Three-dimensional cryoelectron microscopy of dimeric kinesin and ncd motor domains on microtubules. *Proc. Natl. Acad. Sci. USA.* 93:9539–9544.

Howard, J., A. J. Hudspeth, and R. D. Vale. 1989. Movement of microtubules by single kinesin molecules. *Nature.* 342:154–158.

Huang, T-G., J. Suhan, and D. D. Hackney. 1994. Drosophila kinesin motor domain extending to amino acid position 392 is dimeric when expressed in *Escherichia coli. J. Biol. Chem.* 269:16502–16507.

Inoue, Y., Y. Y. Toyoshima, A. H. Iwane, S. Morimoto, H. Higuchi, and T. Yanagida. 1997. Movements of truncated kinesin fragments with a short or an artificial flexible neck. *Proc. Natl. Acad. Sci. USA.* 97: 7275–7280.

Ishijima, A., T. Doi, K. Sakurada, and T. Yanagida. 1991. Sub-piconewton force fluctuations of actomyosin in vitro. *Nature.* 352:301–306.

Ishijima, A., Y. Harada, H. Kojima, T. Funatsu, H. Higuchi, and T. Yanagida. 1994. Single-molecule analysis of the actomyosin motor using nano-manipulation. *Biochem. Biophys. Res. Commun.* 199: 1057–1063.

Ishijima, A., H. Kojima, H. Higuchi, Y. Harada, T. Funatsu, and T. Yanagida. 1996. Multiple- and single-molecule analysis of the actomyosin motor by nanometer-piconewton manipulation with a microneedle: unitary steps and forces. *Biophys. J.* 70:383–400.

Kagami, O., and R. Kamiya. 1992. Translocation and rotation of microtubules caused by multiple species of *Chlamydomonas* inner-arm dynein. *J. Cell. Sci.* 103:653–664.

Kull, F. J., E. P. Sablin, R. Lau, R. J. Fretterick, and R. D. Vale. 1996. Crystal structure of the kinesin motor domain reveals a structural similarity to myosin. *Nature.* 380:550–555.

Kuznetsov, S. A., E. A. Vaisberg, N. A. Shanina, N. N. Magretova, V. Y. Chernyak, and V. I. Gelfand. 1988. The quaternary structure of bovine brain kinesin. *EMBO J.* 7:353–356.

Meyhoefer, E., and J. Howard. 1995. The force generated by a single kinesin molecule against an elastic load. *Proc. Natl. Acad. Sci. USA.* 92:574–578.

Song, Y., and E. Mandelkow. 1993. Recombinant kinesin motor domain binds to β-tubulin and decrates microtubules with a B surface lattice. *Proc. Natl. Acad. Sci. USA.* 90:1671–1675.

Svoboda, K., and S. M. Block. 1994a. Force and velocity measured for single kinesin molecules. *Cell.* 77:773–784.

Svoboda, K., and S. M. Block. 1994b. Biological applications of optical forces. *Annu. Rev. Biophys. Biomol. Struct.* 23:247–285.

Svoboda, K., C. F. Schmidt, B. J. Schnapp, and S. M. Block. 1993. Direct observation of kinesin stepping by optical trapping interferometry. *Nature.* 365:721–727.

Vale, R. D., T. Funatsu, D. W. Pierce, L. Romberg, Y. Harada, and T. Yanagida. 1996. Direct observation of single kinesin molecules moving along microtubules. *Nature.* 380:451–453.

Vale, R. D., T. S. Reese, and M. P. Sheets. 1985. Identification of a novel force-generating protein, kinesin, involved in microtubule-based motility. *Cell.* 42:39–50.

Witman, G. B., J. Plummer, and G. Sander. 1978. *Chlamydomonas* flagellar mutants lacking radial spokes and central tubules. *J. Cell Biol.* 76:729–747.